

Chapter - 3

Experimental and Computational Techniques



Chapter 3

Experimental and Computational Techniques

A tissue is a highly scattering medium. As the light propagates through a tissue, the transmitted light is comprised of three components: unscattered (or coherently scattered), weakly scattered, and multiply scattered light. These different components can be visualized by taking an example of a short pulse of laser light propagating through a tissue.

The coherently scattered light, called the ballistic photons, propagate in the direction of the incoming beam. They, therefore, travel the shortest path and emerge first from the tissue. Ballistic photons carry maximum information on the internal structure of the tissue. The portions of the light that scatter slightly more, but still in the forward direction, are called snake photons because of their wiggly trajectories in the forward direction. These photons are time-delayed with respect to the ballistic photons but still carry significant information on the scattering medium. However, most portions of the light beam undergo multiple scattering and travel long distances within the medium. They emerge even later and are called diffuse photons. They carry little information on the microstructure of the tissue and have to be discriminated in order to image using ballistic and snake photons (1). One of the techniques to isolate the ballistic from diffuse photons is Optical Coherence Tomography (OCT). OCT utilizes an interferometric method to enhance contrast in reflection geometry and has emerged as a

powerful technique for three-dimensional imaging of highly scattering biological media such as a tooth.

Fluorescence microscopy is highly sensitive and the most widely used technique for optical bioimaging (1). It provides a comprehensive and detailed probing of the structure and dynamics for in vitro, as well as in vivo, biological specimens of widely varying dimensions. Fluorescence emission dependent on specific wavelengths of excitation light and the energy of excitation under one photon absorption is greater than the energy of emission (the wavelength of excitation light is shorter than the wavelength of emission light). Fluorescence has the advantage of providing a very high signal-to-noise ratio, which enables us to distinguish spatial distributions of even low concentration species.

3.1 Experimental Technique

For biological applications, it is important to develop instruments, which can collect spectral information rapidly ensuring that the sample remains unchanged by exposure to the intense source. On the other hand, low intensity of signal causes several problems in the fluorescence based experimental techniques. Hence keen understanding of instrumentation is essential for successful application of fluorescence. The description of instrumentation involved in the fluorescence spectroscopy is described here.

3.2 Experimental setup for breast tissue

The experimental setup used in the measurements of breast fluorescence is shown in fig 3.1.

The three major components in the experimental setup are:

- Excitation source
- Spectrometer
- Detection system

3.2 Experimental setup for breast tissue

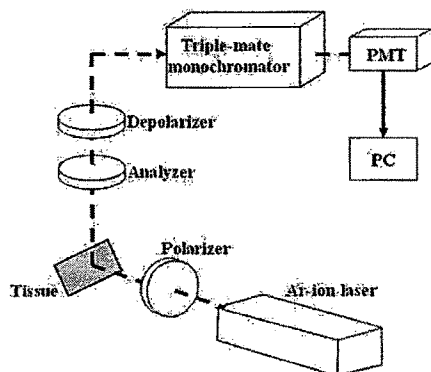


Figure 3.1: Experimental set-up.

3.2.1 Excitation Source (Ar^+ LASER):

For the collection of fluorescence a Spectra Physics Model 165(5W) Argon ion laser is used as an excitation source with the range from UV/Visible wavelength of 457.9nm to the 514nm. It is capable of operating in the TEM_{00} mode at any one of more than 20 spectral lines or at several lines simultaneously. This model consists of the laser head and the Model 265-exciter connected by an 8 feet long umbilical. External thumb wheel controls are provided for wavelength selection and change of intra-cavity aperture. The laser head was designed to a minimum size and weight to take full advantage of the superior operating characteristics of the BeO plasma tube (closed at both ends by Brewster's angle windows). In addition to the plasma tube, laser head contains a solenoid, an optical resonator formed by a spherical reflector at the output end and a prism (for wavelength selection) assisted by a flat mirror at the back end.

The 265 Exciter contains all the necessary electronic circuits to create, sustain and monitor the ion discharge in the plasma tube; to monitor and control the output power; and to supply and regulate the solenoid current. With a start boost circuit (by 7 kV pulse), the exciter generates a discharge in the plasma tube. This exciter contains a fully regulated power supply that controls the ion discharge current in the plasma tube to provide constant laser performance. The

3.2 Experimental setup for breast tissue

Model 165 is designed to use ordinary tap water for cooling of the transistor passbank in the power supply, the magnetic field solenoid and the BeO tube.

NESLAB HX-500 chiller unit provides a continuous flow of de-ionized water at constant temperature (20°C) and pressure (30psi) to the laser head. This is a complete self-contained unit consisting of a stainless steel reservoir, temperature controller, re-circulating pump and refrigeration system. This system design has the ability to track a set temperature virtually independent of changing heat loads. Once the calibrated temperature dial is set, the recalculating temperature will not shift more than a few tenths of a degree. The refrigerator coil immersed in it cools the de-ionized water. It is circulated in a closed loop by the pump. The compressor is water cooled from an external tap.

3.2.2 Spectrometer

In the spectrometer the beam of light is filtered by a double grating, that allows a single wavelength of light to reach the sample. Then in the sample compartment, the sample responds to the incoming radiation. And the resulting radiation is filtered by a double grating emission spectrometer that feeds the signal to a photo multiplier detector. The main parts of this spectrometer are as follows:

3.2.2.1 Lasermate

The 1450 tunable excitation filter is a compact grating monochromator used to eliminate plasma emissions from incident visible laser before the light passes through the sample (3). Figure 3.2 shows the ray diagram for the optical path in the lasermate. This lasermate is attached to the SPEX 1877E triplemate.

3.2.2.2 SPEX 1877E Triplemate

The SPEX 1877 triplemate has two major sections a) the filter stage and b) the spectrograph stage. The filter stage consists of two modified Czerny-Turner 50 mm x 50 mm plane gratings having 600 grooves/mm, coupled in a subtractive mode, and giving a bandpass of about 1000 cm^{-1} on a 5 mm intermediate slit setting. The focal length of the stage is 0.22 m. It acts as a variable wavelength,

3.2 Experimental setup for breast tissue

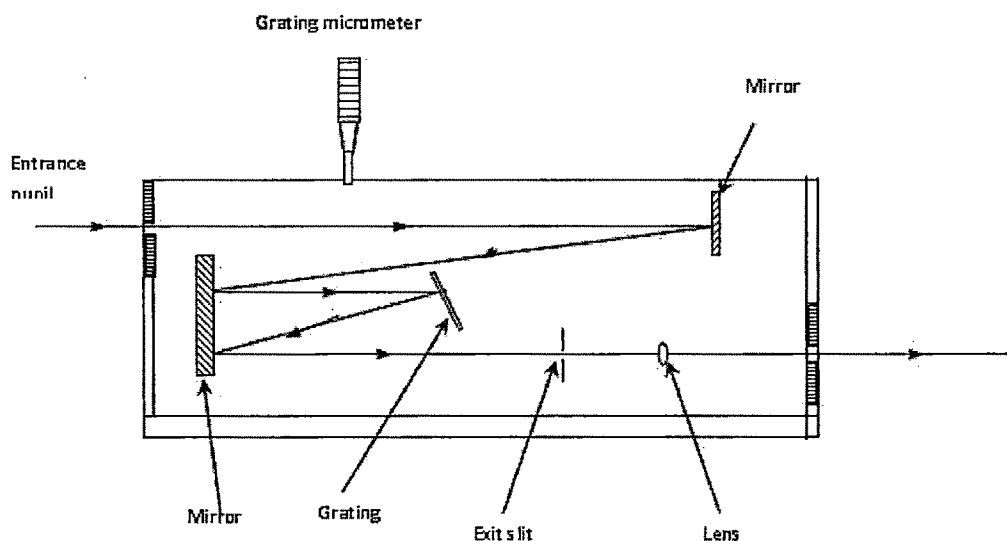


Figure 3.2: Optical diagram of the 1450 tunable excitation filter.

selectable bandpass filter that feeds a non-dispersed segment of radiation from a sample into the entrance slit of spectrograph stage. The spectrograph stage is a 0.6 m, single monochromator which disperses the radiation over the detector. It consists of an asymmetric Czerny-Turner mount with 64mm x 64mm plane grating having 1200 grooves/mm and is used to produce a dispersion of 1.4nm/mm. To vary the dispersion and coverage at the focal plane, the spectrograph has provisions for mounting three gratings of different groove densities on a manually activated turret. The dispersed radiation is then detected by a thermoelectrically cooled PMT.

3.2.3 Detector

The detection system used for the present fluorescence measurement is a photomultiplier tube (PMT), followed by an amplifier, as a photon detector in all fluorimeters. The PMT is a photosensitive device consisting of a photoemissive cathode followed by focusing electrodes, an electron multiplier and an electron collector in a vacuum tube. When light enters the photocathode, the photodiode emits photoelectrons into a vacuum. These are then directed by the focusing

3.3 Experimental setup for cervical tissue

electrodes voltages towards the electron multiplier when electrons are multiplied by the process of secondary emission. The multiplied electrons are then collected by the anode as an output signal. For the detection purpose an end window type RCA C31034 GaAs PMT is used. This PMT has a maximum efficiency in the range 230-880 nm and exceedingly small dark current. The tube is kept at low temperatures (-30°C) using the Peltier effect principle for the best spectral response (6). As the current passes through the thermocouple, the cold junction ultimately reaches -30°C while the hot junction is continuously cooled by flowing tap water. It takes nearly 90 minutes to attain this temperature. The pulse trains from the photomultiplier tube pass through an energy gate (preamp-discriminator), which is designed to discriminate real pulse from spurious ones and amplify them. The data then passes into either a digital photon counter or a suitably interfaced microcomputer fast enough to monitor individual pulses. The output is then recorded in a computer.

3.3 Experimental setup for cervical tissue

The fluorescence spectra of the cervical tissues were recorded using Fluorolog-3 Spectrofluorometer (Jobin Yvon, USA)(2) The block diagram of the experimental setup used is shown in fig.3.3.

The essential parts of fluorometer are:

- Excitation source: Xenon lamp
- Excitation-Emission spectrometer
- Sample compartment
- Detector (PMT, Model: R928)

The output of the detector was connected to computer for data acquisition and analysis.

3.3.1 Excitation Source: Xenon Lamp

The light sources are the high-pressure (10 atmospheres) 450 W Xenon lamps. Xenon lamp (Model 1007) provides a relatively continuous light output from 240nm to 850nm for sample excitation (2). Starting of the lamp requires 20-40

3.3 Experimental setup for cervical tissue

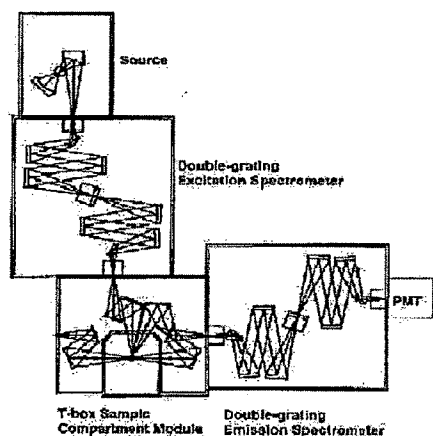


Figure 3.3: Experimental Setup (Fluorolog-3, Model FL3-22).

KV and 25A current. Xenon lamps emit light as a result of the recombination of electrons with ionized Xe ions. The lamp has an approximate life of 2000 hours and is Ozone-free.

3.3.2 Monochromators

A monochromator is an optical device that transmits a mechanically selectable narrow band of wavelengths of light chosen from a wider range of wavelengths available at the input.

Light (A) is focused onto an entrance slit (B) and is collimated by a curved mirror (C). The collimated beam is diffracted from a rotatable grating (D) and the dispersed beam re-focussed by a second mirror (E) at the exit slit (F). Each wavelength of light is focussed to a different position at the slit, and the wavelength which is transmitted through the slit (G) depends on the rotation angle of the grating.

The Fluorolog-3 comes equipped with a double-grating spectrometer in the excitation and emission positions. This is because when a diffraction grating is used, the diffraction pattern has overlapping orders. Sometimes extra, broadband filters are inserted in the optical path to limit the width of the diffraction orders so they do not overlap. This is done by using a prism in one of the monochromators of a dual monochromator design. Double-Grating spectrometers offer a

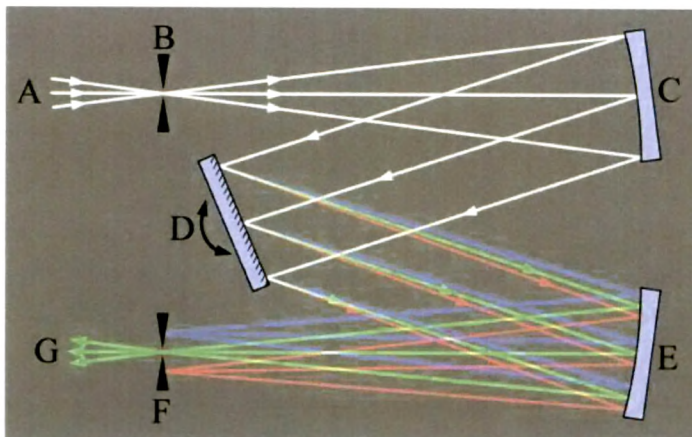


Figure 3.4: Monochromator.

significant increase in sensitivity, resolution and stray-light rejection. In addition, a monochromator includes entrance and exit slits and appropriate mirrors, connected to a small motor which rotate to set the slit's opening as set by the user. In selecting a monochromator for fluorescence spectroscopy, one looks for low stray light levels to avoid problems due to scattered stray light.

Gratings used in this system:

The excitation and emission spectrometer gratings are 1200 groove/mm, measure $50\text{mm} \times 50\text{mm}$ and are blazed at 300nm and 500nm. By definition, a diffraction grating is a piece of polished aluminum onto which a large number of grooves have been etched (typically 10,000 to 15,000 lines/mm).

Slits:

The slits in a fluorescence instrument are used to determine the band pass and have a profound effect on the amount of light that is passed by the monochromator to the next component in the optical system (4). The slit widths are generally variable and a typical monochromator will have both an entrance and exit slit. The light intensity which passes through a monochromator is approximately proportional to square of the slit width (if the slit width is doubled, four times as

3.3 Experimental setup for cervical tissue

much light is passed). Larger slit widths yield increased signal levels, and therefore higher signal-to-noise ratios (5). Smaller slit widths yield higher resolution, but at the expense of light intensity. All the fluorescence spectra were taken at a slit width of 5mm and elastic scattering spectra were taken at a slit width of 1mm of both excitation and emission monochromator.

Sample Compartment:

Fluorescence spectra were measured using a sample holder on which Quartz plate was placed with tissue sample on it. Quartz plate has an advantage that it does not give fluorescence. The standard sample-compartment module is a T-box, which provides efficient throughput with a choice of standard Right Angle (RA) or Front-Face (FF) emission collection. The Fluorescence spectra from solid samples (tissues) were measured in FF geometry (at an angle of 22.5° from the incident direction). This orientation minimizes stray and reflected light off the surface of the sample. In this case the fluorescence signal is collected from the sample's surface. RA detection is used primarily for dilute solutions. The sample compartment module comes equipped with a silicon photodiode reference detector to monitor and compensate variations in the Xenon lamp output.

Detectors: PMT

A photo multiplier tube (PMT) followed by an amplifier is used as a photon detector in all fluorimeters. The PMT is a photosensitive device consisting of a photoemissive cathode followed by focusing electrodes, an electron multiplier and an electron collector in a vacuum tube. When light enters the photocathode, the photodiode emits photoelectrons into a vacuum. These are then directed by the focusing electrodes voltages towards the electron multiplier when electrons are multiplied by the process of secondary emission. The multiplied electrons are then collected by the anode as an output signal. A PMT is best regarded as a source of current, which is proportional to the light intensity. Although a PMT responds to individual photons, these individual pulses are generally detected as an average signal. The PMT is supplied a high voltage of 950 volts to operate in

3.4 Measurement of Fluorescence Polarization

the linear range. The PMT (R 928) is cooled in the room temperature. It can measure Intensity upto 1.6×10^6 cps, and beyond this the PMT saturates.

3.4 Measurement of Fluorescence Polarization

The concept of molecular movement and rotation is the basis of fluorescence polarization. The measurement of polarized emission of fluorescence allows for the observation of rotational motions in fluorophores during the lifetime of excited state. A group of similarly oriented molecules are chosen or photoselected using a polarizer in the excitation path. The polarized components of fluorescence emission are measured using polarizer in the emission path (2). Polarization measurements are performed by measuring the vertically and horizontally polarized components of the emission.

Polarization is defined as the ratio of the linearly polarized component's intensity divided by the natural light component's intensity. In an ideal system, polarization is measured only the vertically polarized excitation with the horizontal and vertical emission components. These measurements are designated as I_{VV} or I_{\parallel} and I_{VH} or I_{\perp} respectively; the first subscript indicating the position of the excitation polarizer and the second subscript indicates the emission polarizer. Vertically oriented polarizers (V) are said to be at 0° (from normal) and horizontal polarizers (H) are said to be at 90° .

Polarization measurements are taken in two geometries, called L and T format. An L-Format polarizer system is shown in figure 3.5. L-format utilizes two polarizers with the emission polarizer rotated between horizontal and vertical polarizations for measurements (2). The entrance and exit polarizers are fully automated and adjustable to within 1° rotations. Insertion and removal of polarizers from the optical path is controlled by the computer. All the Spectra were taken in L-Format polarizer system.

3.4 Measurement of Fluorescence Polarization

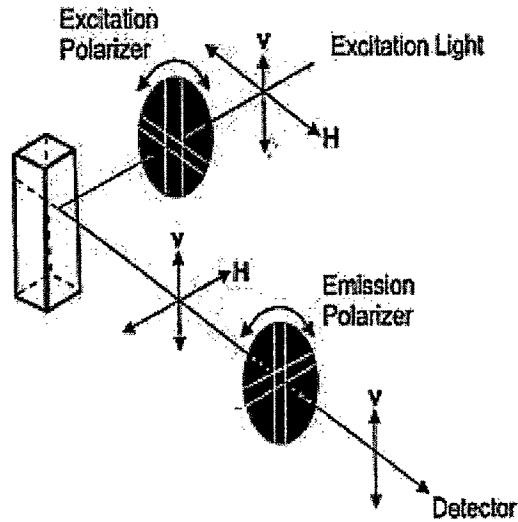


Figure 3.5: L-Format Polarization.

3.4.1 G-Factor:

In a monochromator system, the G factor must be included to correct for the wavelength response to polarization of the emission optics and detectors. A pre-calculated G factor may be used when all other experimental parameters are constant. G factor improves the S/N ratio for weak signals. Polarization measurements that involve scanning the emission monochromator must have the G factor measured for each emission wavelength position. The G factor is defined as:

$$G = G(\lambda_{EM}) = \frac{I_{HV}}{I_{HH}} \quad (3.1)$$

In the experiments performed, measurements of I_{VV} , I_{VH} , I_{HV} , I_{HH} were all taken and finally used in the intrinsic fluorescence model, taking into account the g-factor.

3.5 Material and method

Pathologically characterized fresh Breast and Cervical tissue samples with their normal counterparts were obtained from G.S.V.M. Medical College, Kanpur within two hours of surgery and were kept in refrigerator until used. These were analyzed in close collaboration with the pathologist of the hospital. The age of patients spanned over a broad range, from 16-85 years, coming from varied economic backgrounds. The collected samples were analyzed on the same day, without any chemical treatment. During experiments, the tissue was at room temperature and kept moist with isotonic saline. The tissue was placed on a quartz plate of size $3\text{cm} \times 1\text{cm} \times 2\text{mm}$ during experiment.

The breast samples were excited by 488nm wavelength plane polarized light from an Ar-ion laser and the cervical samples were excited by 350nm from Xenon lamp. The unpolarized and polarized fluorescence spectra were collected in right angle geometry. For polarized fluorescence, a depolarizer was used after the analyzer, in order to ensure that there was no preference of the selected directions of polarized fluorescence by the detection system. The components of fluorescence light which are parallel and perpendicular to the incident polarized light were measured in the 500 to 700nm wavelength region in case of breast tissue and in cervical it was from 380 to 650nm.

The dominant fluorophores in cervical tissue are collagen (peak around 400 nm) and NADH (peak around 460 nm) at excitation wavelength 350 nm. In case of breast tissue FAD (peak around 530 nm) and Porphyrin (peak around 630 nm) are dominant fluorophores for excitation wavelengths 436, 470 and 488 nm. The samples were excited with vertically polarized light and the parallel (both polarizer and analyzer are in same state, VV) and perpendicular (Polarizer and analyzer are in orthogonal state, VH) components of the fluorescence were collected in the reflection geometry. VV is the observed intensity when the observing polarizer is oriented parallel to the direction of the polarized excitation and VH is the observed intensity when the polarizer is perpendicular to the polarized excitation.

3.6 Computational Techniques

3.6.1 Wavelet Transform

Wavelets refer to small waves and wavelet transform refers to the representation of a signal in terms of a finite length or fast decaying oscillating waveform. This waveform, known as the mother wavelet, is scaled and translated to match the input signal. In this representation, a wavelet series, which is the coordinate representation of a square integrable function with respect to a complete, orthonormal set of basis functions for the discrete wavelets under consideration.

The word wavelet is due to Morlet and Grossman in the early 1980s. They used the French word *ondelette*, meaning "small wave". A little later it was transformed into English by translating "onde" into "wave", giving wavelet. Wavelet transforms are broadly classified into the discrete wavelet transform (DWT) and the continuous wavelet transform (CWT). The principal difference between the two is that the continuous transform operates over every possible scale and translation, whereas the discrete ones use a specific subset of all scale and translation values. Furthermore, the discrete wavelet has a strictly finite size.

Wavelet transforms may be considered to be forms of time-frequency representation and are, therefore, related to the subject of harmonic analysis. Almost all practically useful discrete wavelet transforms make use of filter-banks containing finite impulse response filters. The wavelets forming a CWT are subject to Heisenberg's uncertainty principle and equivalently, discrete wavelet bases may be considered in the context of other forms of the uncertainty principle.

3.6.1.1 Multiresolution analysis

Although the time and frequency resolution problems are results of a physical phenomenon (the Heisenberg uncertainty principle) and exist regardless of the transform used, it is possible to analyze any signal by using an alternative approach called the multiresolution analysis (MRA). MRA, as implied by its name, analyzes the signal at different frequencies with different resolutions. Every spectral component is not resolved equally as was the case in the STFT (fig.3.6).

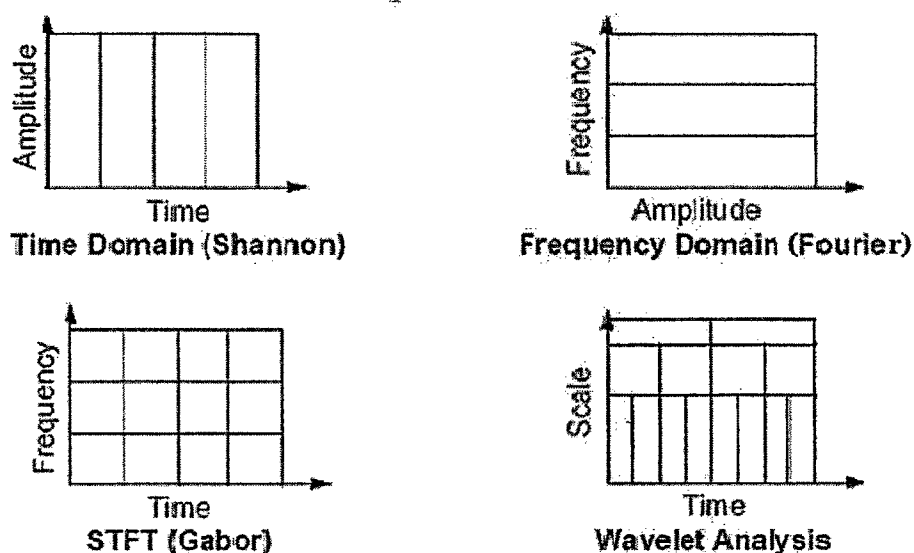


Figure 3.6: Time and frequency resolutions.

MRA is designed to give good time resolution and poor frequency resolution at high frequencies and good frequency resolution and poor time resolution at low frequencies. This approach makes sense especially when the signal at hand has high frequency components for short durations and low frequency components for long durations. Fortunately, the signals that are encountered in practical applications are often of this type. This is the special feature due to which wavelet transform has become so popular.

3.6.1.2 Discrete Wavelet Transform

Wavelet transform is known as mathematical microscope which provides a multi-resolution analysis of the data under consideration. The data is separated into high frequency and low frequency components at multiple scales, known respectively as high pass and low pass coefficients. For example, high pass coefficients at level-1 represent variations at smallest scale and the subsequent higher level coefficients represent variations over bigger window sizes. The low pass coefficients at various levels represent average behavior of data over corresponding window sizes. In discrete wavelet transform (DWT), the basis functions consist of father

wavelet $\phi(x)$ and mother wavelet $\psi(x)$ satisfying

$$\int \phi dx = A, \int \psi dx = 0 \text{ and } \int \phi^* \psi dx = 0. \quad (3.2)$$

ϕ and ψ are also square integrable:

$$\int |\phi|^2 dx = 1 = \int |\psi|^2 dx. \quad (3.3)$$

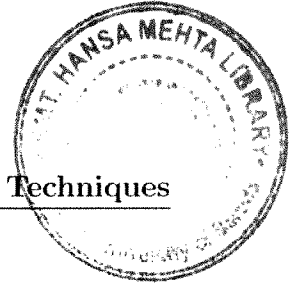
Where, A is an arbitrary constant. Both of these functions belong to the square integrable class. Two operations crucial to the construction of a complete orthonormal basis are translation and scaling. It can be checked that the following scaled and translated wavelets and scaling functions are square integrable;

$$\psi_{j,k} = 2^{j/2} \psi(2^j t - k), \quad (3.4)$$

$$\phi_{j,k} = 2^{j/2} \phi(2^j t - k) \quad (3.5)$$

Here, k is the translation parameter and j is the scaling parameter in the dyadic basis. $2^{j/2}$ is the normalization factor at scale j , which takes integral values starting from zero. The original mother wavelet corresponds to $\psi_{0,0}$ whereas the father wavelet is given by $\phi_{0,0}$. Higher values of j lead to the so called daughter wavelets which are of the similar form as the mother wavelet, except that these are thinner and taller by a factor of $2^{j/2}$. The translation unit $k/2^j$ is also commensurate with the thinner size of the daughter wavelet at scale j . In a given wavelet basis only one scaling function and its translations are taken, since others are not orthogonal to the wavelets. In the above construction the translated scaling functions are given by $\phi_{0,k} \equiv \phi_k = \phi(x - k)$. In the limit $j \rightarrow \infty$ and for integral values of k , in the range $-\infty \leq k \leq \infty$, the above basis becomes a complete set. Hence any finite energy signal $f(t) \in L^2(R)$ (7) can be expanded as

$$f(t) = \sum_{k=-\infty}^{\infty} c_k \phi_k(t) + \sum_{k=-\infty}^{\infty} \sum_{j=0}^{\infty} d_{j,k} \psi_{j,k}(t) \quad (3.6)$$



3.6 Computational Techniques

Explicitly the wavelet coefficients are given by

$$c_{j,k} = \langle f(t), \phi_{j,k}(t) \rangle = \int f(t) \phi_{j,k}(t) dt, \quad (3.7)$$

and

$$d_{j,k} = \langle f(t), \psi_{j,k}(t) \rangle = \int f(t) \psi_{j,k}(t) dt \quad (3.8)$$

Since $\phi_{j,k}$ is a scaling function located at k and having a finite window size commensurate to scale j , $c_{j,k}$ represents the average value of the signal over the same window at location k , $d_{j,k}$, as we will become clear from latter discussions, represent variations of the signal in the same window size. Father wavelets or scaling functions are used for extracting the low frequency, smooth component of the signal. On the other hand the wavelets extract the higher frequency detail component at various scales. Broadly speaking, father wavelets are used for finding the trend components and wavelets pick out the deviations from the trend. All wavelet basis functions satisfy the dilation equation, also known as the multiresolution analysis (MRA) equation(8);

$$\phi(t) = \sum_n h(n) \sqrt{2} \phi(2t - n), \quad (3.9)$$

and

$$\psi(t) = \sum_n \tilde{h}(n) \sqrt{2} \phi(2t - n) \quad (3.10)$$

It is worth noting that both scaling function coefficients (low-pass coefficients) and wavelet coefficients (high-pass coefficients) at a given scale j can be obtained from only low-pass coefficients at a higher scale. As the scale value j increases for fixed k , the scaling function becomes thinner and taller representing approximately a Dirac delta function (fig.3.7). The corresponding low-pass coefficient is then nothing but the sample of the signal at the location k . Hence starting from the samples of the signal at the finest resolution one can obtain all the other scaling function and wavelet coefficients through the MRA equation. One only

needs to know the filter coefficients $h(n)$ and $\tilde{h}(n)$, without explicitly knowing the forms of the wavelet functions. In this sense, wavelet transform is significantly different from Fourier transform.

For the Haar wavelet

$$h(0) = h(1) = 1/\sqrt{2} \quad \text{and} \quad \tilde{h}(0) = -\tilde{h}(1) = 1/\sqrt{2}, \quad (3.11)$$

whereas for the Daubechies-4 basis:

$$h(0) = -\tilde{h}(3) = \frac{1 + \sqrt{3}}{4\sqrt{2}}, \quad h(1) = \tilde{h}(2) = \frac{3 + \sqrt{3}}{4\sqrt{2}}, \quad (3.12)$$

$$h(2) = -\tilde{h}(1) = \frac{3 - \sqrt{3}}{4\sqrt{2}}, \quad \text{and} \quad h(3) = \tilde{h}(0) = \frac{1 - \sqrt{3}}{4\sqrt{2}} \quad (3.13)$$

It is clear that Haar basis is special, since it is the only wavelet which is symmetric and compactly supported and is the simplest one since the interpretation of the wavelet coefficients are quite transparent here; it is also free from artifacts arising due to the finite size of the data. There are infinite varieties of discrete wavelets, the choice of a basis set depends on the application at hand.

The pictorial demonstration of discrete wavelet transform is presented in fig.3.8. $N = 0$ level represents the original signal. In level one i.e., $N = 1$ Haar wavelet decomposition, the nearest neighbor averages and differences are calculated with the normalization factor of $1/\sqrt{2}$, which leaves half of the data in the form of low-pass coefficients and the other half in terms of level-1 high-pass coefficients. Subsequently, the same procedure can be applied once more to the low-pass coefficients to decompose them into level-2 high-pass coefficients and level-2 low-pass coefficients. In total N level decomposition can be carried out.

3.6.1.3 Continuous Wavelet Transform

The continuous wavelet transform was developed as an alternative approach to the short time Fourier transforms to overcome the resolution problem. The wavelet analysis is done in a similar way to the STFT analysis, in the sense that the signal is multiplied with a function, similar to the window function in the STFT, and

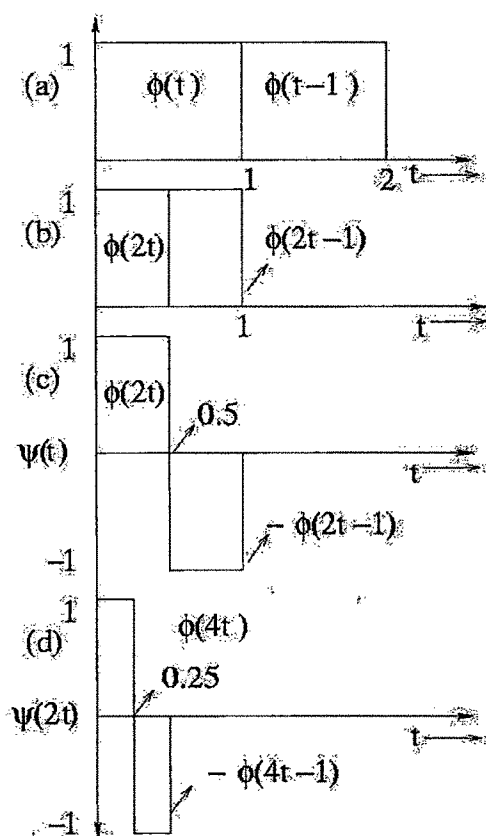


Figure 3.7: Multi-resolution analysis.

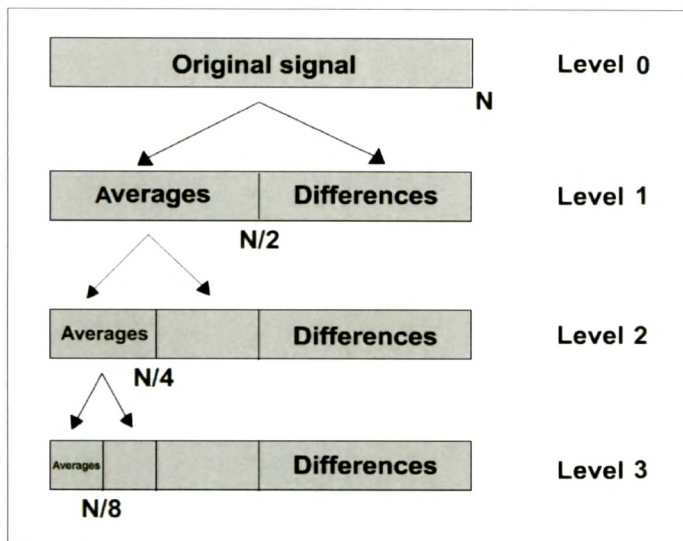


Figure 3.8: Pictorial demonstration of Discrete Wavelet Transform.

the transform is computed separately for different segments of the time-domain signal. However, there are two main differences between the STFT and the CWT:

1. The Fourier transforms of the windowed signals are not taken, and therefore single peak will be seen corresponding to a sinusoid, i.e., negative frequencies are not computed.

2. The width of the window is changed as the transform is computed for every single spectral component, which is probably the most significant characteristic of the wavelet transform.

In the continuous wavelet transform (CWT), a function ψ , which in practice looks like a little wave, is used to create a family of wavelets $\psi(at + b)$, where a and b are real numbers, a dilating (compressing or stretching) the function ψ and b translating (displacing) it (9; 10). In continuous wavelet transform, one uses functions which are smooth, but do not have strictly finite extent. For example, the extensively used Morlet wavelet is a product of a Gaussian function with a cosine: $\psi = c e^{-\frac{t^2}{\sigma}} \cos(\omega t)$; ω and σ (width of the Gaussian) are related (9). The fact that the Gaussian function provides a window to the analyzing function $\cos(\omega t)$, Morlet wavelet closely resembles window Fourier transform, which

allows one to pick out local variations. The Gaussian window can be made small or large by changing the width (scale). It can be translated to identify variations in the data at different locations and at different scales. The continuous wavelets provide an overcomplete basis, as compared to discrete wavelets, which form a complete orthonormal basis. Unlike the smooth Morlet wavelet, the discrete wavelets possess only finite number of derivatives, some of them have fractal character. They are often used to extract variations over average behavior described by a polynomial function. Morlet wavelet is well suited for analyzing the fluorescence spectra containing different fluorophores having Lorentzian line shapes and smooth dips due to absorbers like blood.

The simplest example of an over complete basis can be visualized in a three dimensional Cartesian space. The fact that there are three orthogonal directions X , Y and Z , requires three unit vectors \mathbf{i} , \mathbf{j} & \mathbf{k} along respective directions, to describe an arbitrary vector $\mathbf{A} = a_x\mathbf{i} + a_y\mathbf{j} + a_z\mathbf{k}$. Here, $\mathbf{i}^2 = \mathbf{j}^2 = \mathbf{k}^2 = 1$, $\mathbf{i} \cdot \mathbf{j} = \mathbf{j} \cdot \mathbf{k} = \mathbf{k} \cdot \mathbf{i} = 0$, making these unit vectors an orthogonal basis. a_x , a_y and a_z are components of \mathbf{A} along X , Y and Z directions respectively, and can be obtained by projecting vector \mathbf{A} along these directions, e.g., $a_x = \mathbf{A} \cdot \mathbf{i}$. If more than three unit vectors are used to describe vector \mathbf{A} , the basis is said to be overcomplete. If there are less than three unit vectors then basis set is not complete. As is obvious, an arbitrary vector \mathbf{A} can not be expanded in an incomplete basis. In case of wavelet transform, discrete wavelets form complete orthogonal basis, whereas continuous wavelets are overcomplete. In physical terms, strictly complete basis does not have any redundant information, whereas in overcomplete basis redundancy is present. Often this property is quite useful in pin pointing weak features in data sets thereby making continuous wavelet transform a useful tool for data analysis (9).

In a properly normalized form, the continuous wavelet transform (CWT) of a function $f(t)$, using wavelet ψ , can be written as:

$$CWT_{f(t)}^\psi(\tau, s) = \int f(t) \frac{1}{\sqrt{s}} \psi^*\left(\frac{t-\tau}{s}\right) dt \quad (3.14)$$

As mentioned earlier, the transformed signal is a function of two variables, τ and s , the translation and scale parameters, respectively. The translation pa-

parameter is related to the location of the wavelet window, as the window is shifted through the signal. The scale parameter is defined as 1/frequency and relates to the zooming action of the wavelets. The wavelet coefficients are the function of both scale and wavelength.

3.6.2 Singular Value Decomposition and Principal Component Analysis

Principal Component Analysis (PCA) dimensionally reduces the spectral data into a smaller orthogonal set of linear combinations of the emission variables that account for most of the variance of the spectral data set. Let X denote an $m \times n$ matrix of real-valued data and rank r , (the rank of a matrix is the number of linearly independent rows or columns), where without loss of generality $m \geq n$, and therefore $r \leq n$. The equation for singular value decomposition of X is the following:

$$X = USV^T \tag{3.15}$$

where U is an $m \times n$ matrix, S is an $n \times n$ diagonal matrix, and V^T is also an $n \times n$ matrix. The columns of U are called the left singular vectors, u_k , and form an orthonormal basis for the assay expression profiles, so that $u_i u_j = 1$ for $i = j$, and $u_i u_j = 0$ otherwise. The rows of V^T contain the elements of the right singular vectors, v_k , and form an orthonormal basis for the gene transcriptional responses. The elements of S are only nonzero on the diagonal, and are called the singular values. Thus, $S = \text{diag}(s_1, \dots, s_n)$. Furthermore, $s_k > 0$ for $1 \leq k \leq r$, and $s_i = 0$ for $(r+1) \leq k \leq n$. By convention, the ordering of the singular vectors is determined by high-to-low sorting of singular values, with the highest singular value in the upper left index of the S matrix. Note that for a square, symmetric matrix X , singular value decomposition is equivalent to diagonalization, or solution of the eigenvalue problem.

One way to calculate the SVD is to first calculate V^T and S by diagonalizing $X^T X$:

$$X^T X = VS^2V^T \tag{3.16}$$

3.6 Computational Techniques

and then to calculate U as follows:

$$U = XVS^{-1} \quad (3.17)$$

where the $(r + 1), \dots, n$ columns of V for which $s_k = 0$ are ignored in the matrix multiplication of equation 3.16.

For a square symmetric matrix X , singular value decomposition is equal to diagonalization or solution of the eigenvalue problem. There is a direct relation between PCA and SVD in case where principal components are calculated from the covariance matrix.

For the construction of the empirical correlation matrix C , $\delta I_i(k)$ is computed through mean subtraction of the original values I_i . Here i takes values from 1 to n . Index k represents the sample number. The δI 's have been normalized to have unit variance. Explicitly

$$C_{ij} = \frac{1}{N} \sum_{k=1}^N \delta I_i(k) \delta I_j(k) \quad (3.18)$$

Here, $A_{ik}^T = \delta I_i(k)$ and correlation matrix is of the form $C = (A^T A)/N$.

If the correlation matrix is derived from random numbers (11) the corresponding eigenvalues have maximum and minimum values given by (12):

$$\lambda_{min}^{max} = \sigma^2 (1 + 1/Q \pm 2\sqrt{1/Q}) \quad (3.19)$$

Here, σ^2 is the variance (1 for the present case) and $Q = n/N$. All the eigenvalues λ lie between λ_{min} and λ_{max} with a density ρ of the form:

$$\rho_C(\lambda) = \frac{Q}{2\pi\sigma^2} \frac{\sqrt{(\lambda_{max} - \lambda)(\lambda - \lambda_{min})}}{\lambda} \quad (3.20)$$

3.6.3 Autocorrelation

Autocorrelation is one of the commonly used tool for time series analysis and is employed mainly to detect periodicity buried under noise. As the name suggests, auto-correlation measures the degree of correlation present in a time series with itself, over different time scales. Measuring the correlation between observations of a given time series as a function of their temporal differences gives an estimate as to whether there is any underlying recurrence pattern in the signal, and if so, what is the period of such recurrence. The autocorrelation of a discrete process denoted by X_t for $t = 1, 2, \dots, N$, can be represented as,

$$R(\tau) = 1/(N - \tau - 1) \sum_{t=1}^{N-\tau} (X_t - \mu_1)(X_{t+\tau} - \mu_2)/\sigma_1\sigma_2 \quad (3.21)$$

where $R(\tau)$ denotes the correlation for lag τ lying within the range $[0, \tau_{max}]$, N is the length of the time series, the value of maximum lag allowed τ_{max} is chosen as $3N/4$, μ_1 denotes the mean of the first half of the time series ranging from X_1 to $X_{N-\tau}$, μ_2 denotes the mean of the other half of the time series ranging from $X_{1+\tau}$ to X_N , whereas σ_1 and σ_2 are corresponding standard deviations of the two halves. Note that for τ equal to zero, we are basically measuring the correlation of a time series with itself, hence for lag zero, the value of autocorrelation would be one.

3.6.4 Kernel-Smoother (ks) density

Kernel density estimation is a non-parametric way of estimating the probability density function of a random variable.

A kernel is a non-negative real-valued integrable function K satisfying the following two requirements:

$$\int_{-\infty}^{+\infty} K(u)du = 1; \quad (3.22)$$

$$K(-u) = K(u) \text{ for all values of } u. \quad (3.23)$$

3.6 Computational Techniques

The first requirement ensures that the method of kernel density estimation results in a probability density function. The second requirement ensures that the average of the corresponding distribution is equal to that of the sample used.

If K is a kernel, then so is the function K^* defined by $K^*(u) = \lambda^{-1}K(\lambda^{-1}u)$, where $\lambda > 0$. This can be used to select a scale that is appropriate for the data.

If $x_1, x_2, \dots, x_n \sim f$ is an independent and identically-distributed sample of a random variable, then the kernel density approximation of its probability density function is

$$\hat{f}_h(x) = \frac{1}{nh} \sum_{i=1}^n K\left(\frac{x - x_i}{h}\right) \quad (3.24)$$

where K is some kernel and h is a smoothing parameter called the bandwidth. Quite often K is taken to be a standard Gaussian function with mean zero and variance 1. Thus the variance is controlled indirectly through the parameter h :

$$K\left(\frac{x - x_i}{h}\right) = \frac{1}{\sqrt{2\pi}} e^{-\frac{(x-x_i)^2}{2h^2}} \quad (3.25)$$

References

- [1] P. N. Prasad, *Introduction to Biophotonics*, Wiley Interscience. 36, 37
- [2] Fluorolog-3 (Model FL3-22) operation Manual, Jobin Yvon, Horiba, USA. 41, 45
- [3] Instruction Manual, 1450 Tunable Excitation Filter (Spex Industries Inc. USA). 39
- [4] G. G. Guilbault, "Practical Fluorescence", (1983). 43
- [5] J. R. Lakowicz, "Principles of Fluorescence Spectroscopy", Plenum Press, (1983). 44
- [6] M. Cole and D. Ryer, "Cooling PM tubes for best spectral response", *Electro optical systems design, Milton S. kiver publ.*, 16, (1972). 41
- [7] C. Chui, *An Introduction to Wavelets* (Academic press, New York, 1992). 50
- [8] S. G. A. Mallat, IEEE Transactions on Pattern Analysis and Machine Intelligence **11**, **7**, (1989). 51
- [9] I. Daubechies, *Ten Lectures on Wavelets*, (CBMS-NSF regional conference series in applied mathematics, Philadelphia, PA, 1992, Vol. 64). 54, 55
- [10] B. B. Hubbard, *The World According to Wavelets*, 2nd edition, University Press (India), Hyderabad, (2003). 54
- [11] N. Mehta, *Random Matrices*, (Academic Press, New York, 1995). 57
- [12] A. M. Sengupta and P. P. Mitra, "Distributions of singular values for some random matrices", *Phys. Rev. E*, **60**, 3389, (1999). 57